

THE GAIA-WISE EXTRAGALACTIC ASTROMETRIC CATALOG

JENNIE PAINE,¹ JEREMY DARLING,¹ AND ALEXANDRA TRUEBENBACH¹

¹*Center for Astrophysics and Space Astronomy
Department of Astrophysical and Planetary Sciences
University of Colorado, 389 UCB
Boulder, CO 80309-0389, USA*

Submitted to ApJ

ABSTRACT

The *Gaia* mission has detected a large number of active galactic nuclei (AGN) and galaxies, but these objects must be identified among the 1000-fold more numerous stars. Extant astrometric AGN catalogs do not have the uniform sky coverage required to detect and characterize the all-sky low-multipole proper motion signals produced by the barycenter motion, gravitational waves, and cosmological effects. To remedy this, we present an all-sky sample of 567,721 AGN in *Gaia* Data Release 1, selected using WISE two-color criteria. The catalog has fairly uniform sky coverage beyond the Galactic plane, with a mean density of 12.8 AGN per square degree. The objects have magnitudes ranging from $G = 8.8$ down to *Gaia*'s magnitude limit, $G = 20.7$. The catalog is approximately 50% complete but suffers from low stellar contamination, roughly 0.2%. We predict that the end-of-mission *Gaia* proper motions for this catalog will enable detection of the secular aberration drift to high significance (23σ) and will limit the anisotropy of the Hubble expansion to about 2%.

Keywords: astrometry — catalogs — galaxies: active — infrared: galaxies — proper motions — quasars: general

1. INTRODUCTION

The *Gaia* mission will provide astrometric and proper motion measurements for a large number of bright active galactic nuclei (AGN), but separating the $\sim 10^6$ extragalactic objects from the $\sim 10^9$ stars remains challenging (Gaia Collaboration et al. 2016). Current catalogs include the Large Quasar Astrometric Catalog (LQAC; Souchay et al. 2015), the Véron Catalog of Quasars and AGN (Véron-Cetty & Véron 2010), the Secrest et al. (2015) catalog of mid infrared AGN, and the *Gaia* Universe Model Snapshot (GUMS), a simulated catalog (Robin et al. 2012). Many of these catalogs are dominated by the Sloan Digital Sky Survey (SDSS) footprint that covers 35% of the sky (Ahn et al. 2012), which is problematic for all-sky proper motion studies that attempt to detect low-multipole correlated proper motion signals such as the secular aberration drift dipole (Titov & Lambert 2013; Xu et al. 2012; Truebenbach & Darling 2017), the stochastic gravitational wave background quadrupole (Gwinn et al. 1997; Titov et al. 2011; Book & Flanagan 2011; Darling et al. 2017), or the isotropy of the Hubble expansion (Darling 2014; Chang & Lin 2015; Bengaly 2016).

Desirable features of extragalactic proper motion catalogs are all-sky, uniform selection, and low stellar contamination. Completeness is not very important: it impacts the signal-to-noise of correlated global proper motions, which scales with the square root of the number of objects. In this work, we consider only low-multipole proper motion signals, but completeness will ultimately determine the maximum multipole that can be studied due to the limiting sky density of sources. Stellar contamination is the largest concern for detecting global signals of a few $\mu\text{arcsec yr}^{-1}$ because stellar proper motions can be large and significant and therefore dominate the individually non-significant extragalactic proper motions. What stellar contamination remains in any given extragalactic catalog may be addressed using a non-Gaussian permissive likelihood function as described in Darling et al. (2017).

This paper presents the *Gaia*-WISE extragalactic astrometric catalog, a catalog designed to have low stellar contamination and fairly uniform sky coverage outside of the Galactic Plane. Section 2 presents the WISE color-color selection used to identify AGN and exclude stars, and Section 3 explores the sky distribution of the catalog, its optical and mid-IR properties, its redshift distribution, and the expected end-of-mission proper motion uncertainties. Section 4 predicts the performance of this catalog in detecting the secular aberration drift caused by the barycenter acceleration about the Galactic Center. Section 4 also predicts the expected *Gaia* sensitivity to anisotropy in the Hubble expansion. We discuss the ramifications of this work and the future prospects for extragalactic proper motion studies in Sections 5 and 6. We assume a Hubble constant of $H_0 = 72 \text{ km s}^{-1} \text{ Mpc}^{-1}$

and a flat cosmology (other cosmological assumptions are not required).

2. CATALOG SELECTION METHOD

The WISE survey is an all-sky mid-infrared (MIR) survey in the 3.4, 4.6, 12 and 22 μm bandpasses (W1, W2, W3, and W4, respectively; Wright et al. 2010). The *AllWISE* data release, used in this work, combines data from the cryogenic and post-cryogenic (Mainzer et al. 2011) survey phases, and provides better sensitivity and accuracy over previous WISE data releases. WISE colors have been shown to cleanly separate AGN from stars and normal galaxies, and several methods exist in the literature for selecting AGN with WISE (e.g. Assef et al. 2013; Mateos et al. 2012; Stern et al. 2005, 2012; Truebenbach & Darling 2017). To create our catalog of *Gaia* AGN, we did not consider selection methods using only a W1-W2 color cut in order to avoid contamination from brown dwarfs at low Galactic latitudes, which can reside in the color space selected by single color cuts (Kirkpatrick et al. 2011).

We employed the ALLWISE catalog of MIR AGN described in Secrest et al. (2015). The catalog is based on the WISE two color selection technique of Mateos et al. (2012) which has cuts in the W1-W2 and W2-W3 color space, referred to as the color wedge. This AGN color wedge was defined based on the Bright Ultrahard *XMM-Newton* survey (BUXS), one of the largest flux-limited samples of ‘ultrahard’ X-ray-selected AGN, but the method does not employ X-ray selection directly. BUXS is comprised of 258 objects, of which 56.2% are type 1 AGN and nearly the rest are type 2. BUXS type 2 AGN are intrinsically less luminous than type 1 AGN. Since the completeness of the MIR wedge has a strong dependence on luminosity, the wedge preferentially selects type 1 AGN. Secrest et al. (2015) selected 1.4 million MIR AGN using ALLWISE profile fitting magnitudes with $S/N \geq 5$ and the color wedge criteria of Mateos et al. (2012). They included an additional constraint of limiting to ALLWISE sources with `cc_flags` = “0000” to avoid sources contaminated by image artifacts.

We cross-matched the Secrest et al. (2015) catalog of MIR AGN with *Gaia* Data Release 1 using *allwise_best_neighbour*, the precomputed WISE cross-match table provided in the *Gaia* archive (Marrese et al. 2017). The table includes only the most likely matches between the WISE and *Gaia* catalogs, called “best neighbours.” Since *Gaia* is used as the leading catalog in cross-matching, a *Gaia* source may be matched to multiple sources from an external catalog. Marrese et al. (2017) then determine the best match to the *Gaia* source using the angular distance, position errors, epoch difference, and density of sources in the external catalog. A small number of *Gaia* sources have $G > 21$, fainter than *Gaia*’s nominal magnitude limit of 20.7, which are likely incorrectly determined magnitudes

(Gaia Collaboration et al. 2016). Such objects were excluded from the cross-match. Additionally, all stars from the Tycho 2 survey were removed to avoid stellar contamination, which excluded 65 objects. We discuss possible further stellar contamination in Section 2.2. The resulting catalog of *Gaia* MIR AGN contains 567,721 objects. The first ten objects are given in Appendix A, and the full catalog is available online.

2.1. Completeness

The completeness of the WISE color wedge selection is dependent on the ratio of the AGN luminosity to the host luminosity because host galaxy light can contaminate the MIR emission (Mateos et al. 2012; Padovani et al. 2017). Thus, lower luminosity AGN will have colors of normal galaxies and will be excluded by the color wedge. To assess the completeness of our catalog, we compared the catalog to the sample of SDSS DR9 QSOs (Ahn et al. 2012) in *Gaia*. SDSS QSOs were identified in the *Gaia* source catalog via the cross-matching algorithm provided in the *Gaia* archive with a matching radius of 1 arcsecond. 44.6% of all *Gaia*-SDSS QSOs were also identified by the WISE color wedge, suggesting that our sample is missing more than half of all AGN in the *Gaia* catalog. Only 49.3% of *Gaia*-SDSS QSOs have S/N > 5 detections and zero contamination and confusion flags in all three WISE bands; most of the incompleteness of the *Gaia*-WISE catalog is therefore due to non-detections in the least-sensitive WISE W3 band. Among the WISE-detected *Gaia*-SDSS QSOs, 90.2% lie in the WISE MIR color wedge. The remaining quasars generally have bluer W1–W2 colors than the color wedge, likely due to contamination by host galaxy starlight.

2.2. Stellar Contamination

Mateos et al. (2012) find that contamination by normal galaxies in the MIR wedge is minimal. For astrometric purposes, however, objects need only be extragalactic, so unresolved galaxies are acceptable. Contamination by Galactic stars is of much greater concern due to their large proper motions.

To assess any remaining stellar contamination after omitting the Tycho stars, we cross matched our sample with the SDSS DR12 catalog (Alam et al. 2015). 229,073 AGN in our sample reside within the SDSS footprint, and 65,575 have a spectroscopic classification from SDSS. Of those, only 104 objects (0.16%) are identified by their spectroscopic classification as stars. Extrapolating to the whole sky gives approximately 910 total stars in our sample, suggesting negligible contamination from stars. We also consider contamination from dusty stars that would not be found in our SDSS cross-match. Nikutta et al. (2014) find that a majority of objects brighter than W1 = 11 are Galactic stars. Our sample contains 1,836 objects with W1 < 11, which in-

dicates a maximum of 0.32% contamination from dusty stars.

3. RESULTS

3.1. Sky Distribution

Figure 1 illustrates the distribution of *Gaia*-WISE AGN on the sky. The lower density of AGN at low Galactic latitudes is due to a combination of dust along the Galactic plane and the effectiveness of the MIR color wedge at excluding stars. Additionally, WISE photometry is limited by confusion near the Galactic plane due to high source density (Wright et al. 2010). The higher densities near the ecliptic poles are due to increased coverage by both WISE and *Gaia*. The mean and median densities above the Galactic plane ($b > 15^\circ$) are 12.8 and 12.0 objects per deg², respectively, and the maximum density is 55 objects per deg².

3.2. Optical Properties

Gaia surveys the sky down to $G = 20.7$, with a small fraction of objects at $G > 21$ (Gaia Collaboration et al. 2016). As illustrated in Figure 2, the majority of WISE AGN lie at the fainter end of *Gaia*'s magnitude distribution. Statistics for the distribution of G magnitudes are listed in Table 1.

3.3. Mid-IR Properties

The WISE two color distribution for our catalog is shown in Figure 3, along with the Mateos et al. (2012) wedge. The majority of objects reside in a locus near the bluer end of the color wedge, with a small number of outliers with redder colors. The distribution around the locus tapers before the color cuts, suggesting that the color wedge captures most of the AGN population, except for the bottom right cut where AGN colors begin to overlap with the color space occupied by normal galaxies. The distributions of WISE W1, W2, and W3 magnitudes, and W1–W2 and W2–W3 colors are shown in Figure 4; statistics for these distributions are given in Table 1.

3.4. Redshifts

Redshifts were obtained for objects with spectroscopic redshifts from SDSS. Redshifts with nonzero warning flags or negative errors were discarded, since a negative redshift error indicates a poor fit even if the warning flag is zero. This yielded redshifts for 90,365 objects ($\sim 15\%$). Note that this distribution is incomplete and subject to selection bias due to targeted quasar surveys by SDSS and the redshift sensitivity biases thereof. The catalog contains 202 redshifts above $z = 4$, which is unexpectedly high considering *Gaia*'s magnitude limit. However, a majority of these are confirmed quasars in the SDSS Baryon Oscillation Spectroscopic Survey (BOSS) quasar catalog, of which many were selected for the survey using WISE colors (Pâris et al. 2017).

Table 1. Catalog Statistics

	G	W1	W2	W3	W1–W2	W2–W3	Redshift	$\sigma_{\mu, RA}^a$	$\sigma_{\mu, Dec}^a$
	(mag)	(mag)	(mag)	(mag)	(mag)	(mag)		($\mu\text{as yr}^{-1}$)	($\mu\text{as yr}^{-1}$)
Mean	19.3	15.2	14.0	10.9	1.2	3.0	1.3	236	218
Median	19.4	15.3	14.1	11.1	1.2	3.0	1.2	205	191
Minimum	8.8	4.8	3.7	0.2	0.5	2.0	0.0	2	3
Maximum	21.0	18.8	17.1	12.9	2.2	5.8	7.0	1062	797

^a *Gaia* expected end-of-mission proper motion uncertainty (see Section 3.5).

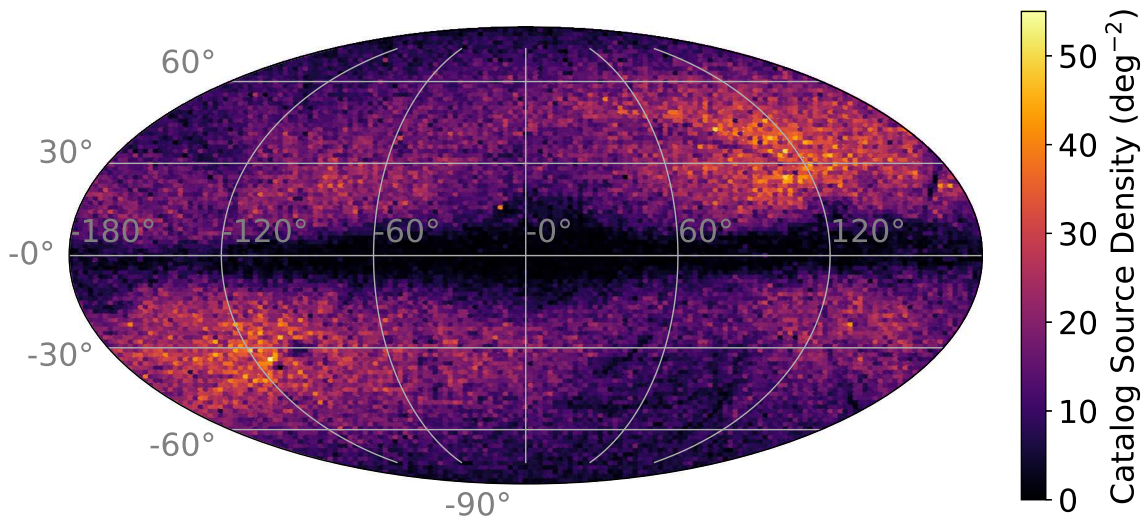


Figure 1. *Gaia*-WISE extragalactic astrometric catalog density plot in Galactic coordinates. The colorbar indicates the number of objects per deg^2 .

3.5. Proper Motion Uncertainties

Gaia DR2 will include positions, proper motions, and parallaxes — or limits on these quantities — for all objects. Predicted proper motion standard errors can be calculated ahead of the release using *Gaia* performance characteristics.¹ The PyGaia Python toolkit is an implementation of *Gaia* performance models that can be used for basic simulation and analysis of *Gaia* data, including calculation of proper motion uncertainties. We utilized the PyGaia Python toolkit to calculate predicted proper motion uncertainties for each AGN, shown in Figure 6. This calculation relies on each object’s G magnitude, $V - I_C$ color, and ecliptic latitude. For objects where the $V - I_C$ color was not available, this value was set to zero, which has a negligible impact on the predicted proper motion uncertainty. The reported uncertainties include known instrumental effects. Statistics for the distributions of predicted uncertainties are given in Ta-

ble 1. The uncertainties in right ascension proper motion are generally larger than in declination, which is a consequence of the *Gaia*’s scanning law.

4. APPLICATIONS

Although proper motions for *Gaia* AGN will not be available until DR2, we can use the predicted uncertainties to test *Gaia*’s potential capability to detect or constrain select proper motion signals. For this purpose, we generate a null proper motion catalog by randomly selecting proper motions consistent with zero based on each object’s expected errors and assuming Gaussian-distributed errors. One can then add proper motion signals to the noisy null catalog to study the expected sensitivity of the *Gaia*-WISE catalog to various correlated proper motions. These include the secular aberration drift (Section 4.1), an anisotropic Hubble expansion (Section 4.2), and a stochastic long-period gravitational wave background (Darling et al. 2017).

4.1. Secular Aberration Drift

¹ www.cosmos.esa.int/web/gaia/science-performance

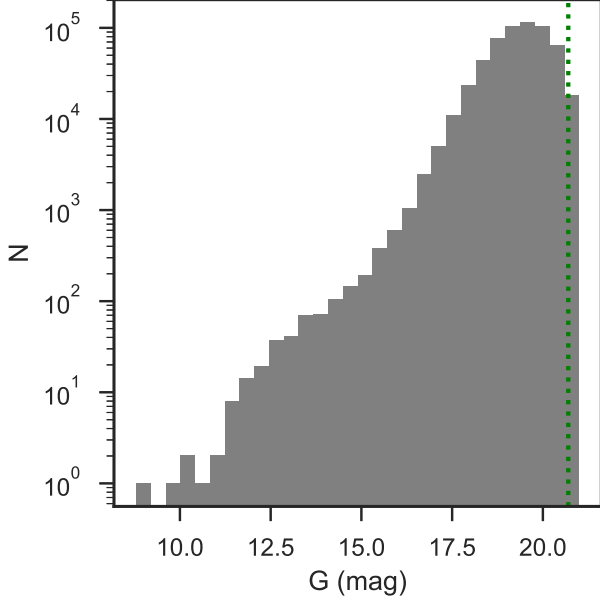


Figure 2. Distribution of *Gaia* G-band magnitudes in the *Gaia*-WISE extragalactic astrometric catalog. The green dotted line indicates *Gaia*'s nominal magnitude limit, $G = 20.7$.

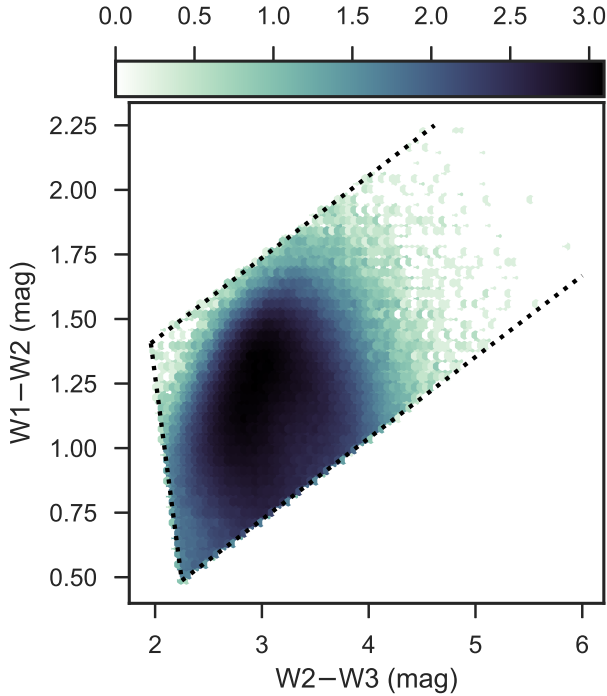


Figure 3. WISE colors for *Gaia* MIR AGN. The dashed lines indicate the color wedge of Mateos et al. (2012). The color bar indicates the logarithm of the number of objects per hexagonal bin.

The aberration of light is an apparent angular deflection of light rays caused by an observer's velocity across the rays and the finite speed of light. Aberration can be caused by the Earth's annual motion or the secular Solar motion in the Galaxy or with respect to the cosmic microwave background rest frame. If the observer experiences a constant acceleration then the aberration will exhibit a secular drift that manifests as an apparent proper motion of objects in a dipole pattern converging toward the acceleration vector direction.

The secular aberration drift caused by the solar system's acceleration toward the Galactic Center (a consequence of its orbit) is detectable in extragalactic proper motions as a dipole vector field that resembles an electric field and converges on the Galactic Center (e.g. Xu et al. 2012; Titov & Lambert 2013; Truebenbach & Darling 2017). The expected solar acceleration and corresponding secular aberration drift dipole amplitude can be predicted using the distance to the Galactic center (R_0) and the orbital speed of the Sun ($\Theta_0 + V_\odot$), which includes solar motion V_\odot in the direction of Galactic rotation Θ_0 : $a = (\Theta_0 + V_\odot)^2 / R_0$ and $|\vec{\mu}| = a/c$. Reid et al. (2014) measured $R_0 = 8.34 \pm 0.16$ kpc and $\Theta_0 + V_\odot = 255.2 \pm 5.1$ km s $^{-1}$ from the trigonometric parallaxes and proper motions of masers associated with young massive stars. These yield an acceleration of $a = 0.80 \pm 0.04$ cm s $^{-1}$ yr $^{-1}$ and a dipole amplitude of $|\vec{\mu}| = 5.5 \pm 0.2$ μ as yr $^{-1}$.

An E-mode vector field dipole painted on the sky, $\tilde{\mathbf{V}}_{E1}(\alpha, \delta)$, can be expressed as a $\ell = 1$ vector spherical harmonic following the notation of Mignard & Klioner (2012):

$$\begin{aligned} \tilde{\mathbf{V}}_{E1}(\alpha, \delta) = & \left(s_{11}^{Re} \frac{1}{2} \sqrt{\frac{3}{\pi}} \sin \alpha + s_{11}^{Im} \frac{1}{2} \sqrt{\frac{3}{\pi}} \cos \alpha \right) \hat{\mathbf{e}}_\alpha \\ & + \left(s_{10} \frac{1}{2} \sqrt{\frac{3}{2\pi}} \cos \delta + s_{11}^{Re} \frac{1}{2} \sqrt{\frac{3}{\pi}} \cos \alpha \sin \delta \right. \\ & \left. - s_{11}^{Im} \frac{1}{2} \sqrt{\frac{3}{\pi}} \sin \alpha \sin \delta \right) \hat{\mathbf{e}}_\delta \end{aligned}$$

where the coefficients $s_{\ell m}^{Re, Im}$ determine the direction and amplitude of the dipole, α and δ are the right ascension and declination coordinates, and $\hat{\mathbf{e}}_\alpha$ and $\hat{\mathbf{e}}_\delta$ are the unit vectors in those directions. In this formalism, the expected E-mode dipole caused by the solar orbit about the Galactic Center (266.4° , -29.0°) is $(s_{10}, s_{11}^{Re}, s_{11}^{Im}) = (-7.71 \pm 0.34, 0.615 \pm 0.027, -9.82 \pm 0.44)$ μ as yr $^{-1}$.

In order to predict the *Gaia* sensitivity to the secular aberration drift signal, we assigned a proper motion to each object that is consistent with no proper motion by randomly sampling its predicted Gaussian proper motion error distribution (Section 3.5). Over 1000 random trials, we added the expected secular aberration drift signal to the noisy null proper motions, omitting the uncertainties in the input dipole, and used a least squares

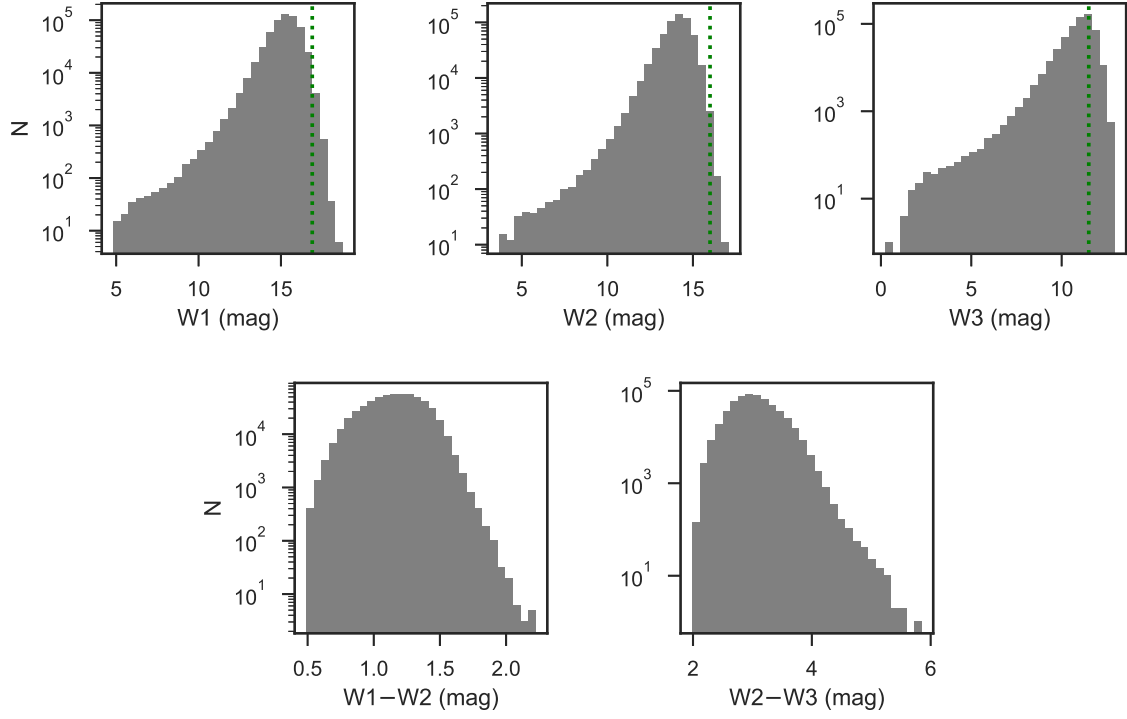


Figure 4. Distribution of W1, W2, and W3 band magnitudes, and W1–W2 and W2–W3 colors in the *Gaia*-WISE extragalactic astrometric catalog. Green dotted lines show the nominal S/N = 5 magnitudes for each band (16.9, 16.0, and 11.5 for W1, W2, and W3, respectively).

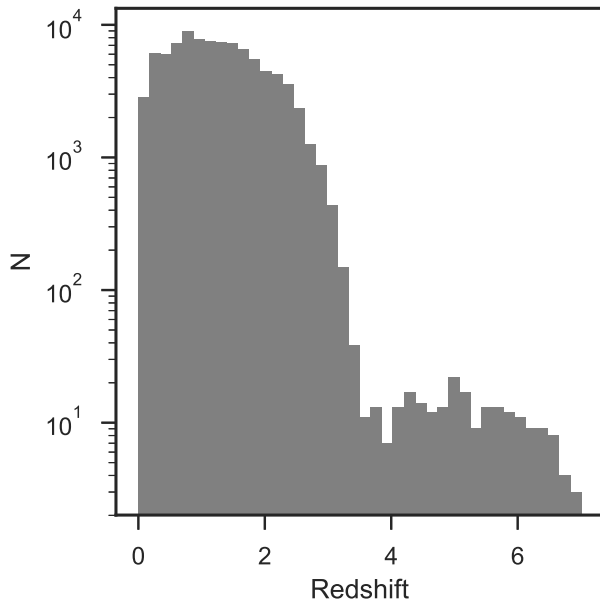


Figure 5. Distribution of redshifts in the *Gaia*-WISE extragalactic astrometric catalog, where available (Section 3.4).

minimization to fit a dipole to the data. The resulting mean of the best fit parameters is $(s_{10}, s_{11}^{Re}, s_{11}^{Im}) = (-7.73 \pm 0.48, 0.606 \pm 0.337, -9.79 \pm 0.36) \mu\text{as yr}^{-1}$, con-

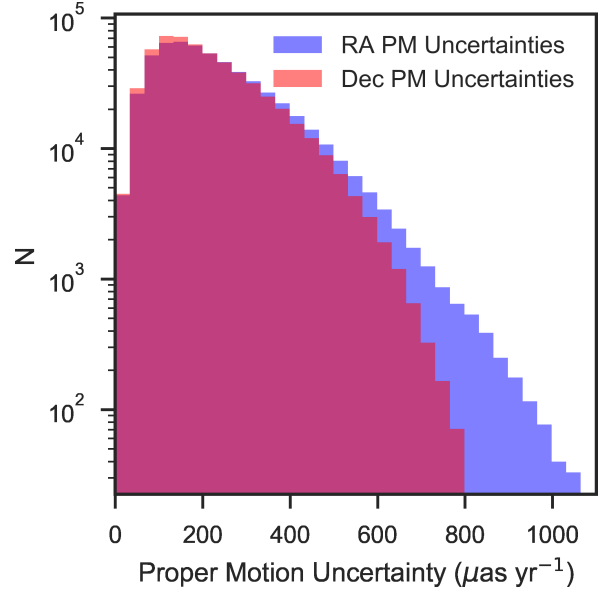


Figure 6. Predicted proper motion uncertainties in both right ascension (blue) and declination (pink), with overlapping values shown in magenta.

sistent with the original input dipole, with mean Z-score of 23. We therefore predict that *Gaia* will produce

the best determination of the secular aberration drift to date.

4.2. Anisotropic Cosmic Expansion

Extragalactic proper motions can test the isotropy of the Hubble expansion in the current epoch. If we neglect the peculiar motions of galaxies caused by density inhomogeneities, an isotropic Hubble expansion produces no extragalactic proper motions. In contrast, anisotropic expansion will cause extragalactic objects to stream toward directions of faster expansion and away from directions with slower expansion. All-sky proper motion observations can therefore measure the expansion isotropy and constrain cosmological models that attempt to explain accelerating expansion without invoking dark energy, such as Lemaitre-Tolman-Bondi models and Bianchi universes (e.g. [Amendola et al. 2013](#)).

[Quercellini et al. \(2009\)](#) and [Fontanini et al. \(2009\)](#) showed that a triaxial expansion can be described using a Bianchi I model, which has the metric

$$ds^2 = -dt^2 + a^2(t) dx^2 + b^2(t) dy^2 + c^2(t) dz^2. \quad (1)$$

This metric permits different expansion rates along the three axes: $H_x = \dot{a}/a$, $H_y = \dot{b}/b$, and $H_z = \dot{c}/c$. The observed Hubble parameter would be $H = \frac{d}{dt}(abc)^{1/3}/(abc)^{1/3}$, and the Friedmann-Robertson-Walker metric is recovered for $a(t) = b(t) = c(t)$. The expansion can therefore be characterized by the fractional departure from the isotropic Hubble expansion along the coordinate i using a unitless shear parameter:

$$\Sigma_i = \frac{H_{i,0}}{H_0} - 1. \quad (2)$$

The principal shearing axes can be arbitrarily oriented on the sky, and [Darling \(2014\)](#) showed that the proper motion induced by this anisotropy model can be completely described by a quadrupolar E-mode vector field.

To test the catalog’s potential to constrain anisotropy, we performed 1,000 trials of adding a randomly generated anisotropy signal to the noisy null proper motions and fitting the anisotropy model to attempt to recreate the original input signal. We used the shear equation (Equation A1) of [Darling \(2014\)](#) to form these artificial anisotropy signals. For each trial, shear terms Σ_x , Σ_y , and Σ_z were drawn from Gaussian distributions with mean of zero and random standard deviation sampled from a uniform distribution between 0 and 0.1. The rotation angles were randomly selected from a uniform distribution between 0 and 2π , assuming that there is no preferred direction for anisotropy. After the signal is added to the null proper motions, we use a least squares minimization to fit the shear equation to the data in an attempt to recover the original signal.

The shear equation parameters are degenerate due to the rotation degeneracy of the principal axes (no particular axis is required to be the direction of maximum or

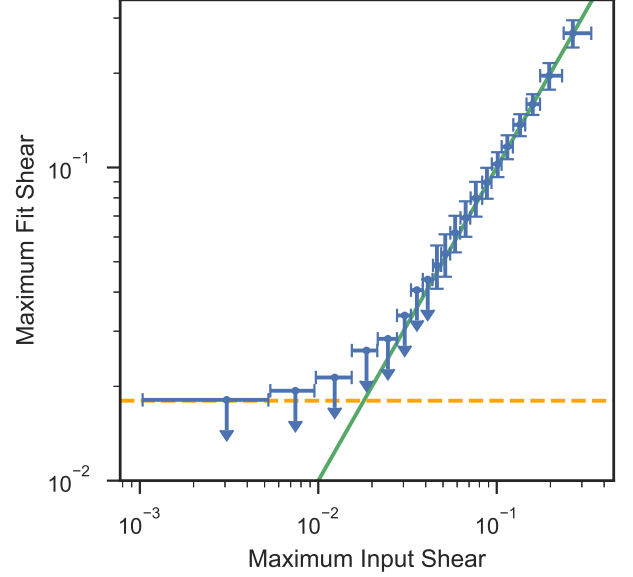


Figure 7. Maximum absolute value of the fit shear vs. the input shear for Hubble expansion anisotropies added to the synthetic *Gaia*-WISE AGN catalog proper motions. Non-significant fits are displayed as upper limits.

minimum expansion), and therefore individual fit parameters do not necessarily match the original input parameters. Instead, we compare the maximum input shear to the maximum fit shear, as shown in Figure 7. There is a roughly one-to-one correlation for large input values; however, for maximum input shear below $\sim 3 \times 10^{-2}$, noise dominates and the fit parameters tend toward a noise floor of 0.018 (a 1.8% departure from anisotropy). The fit, however, is not significant for such low input anisotropy.

5. DISCUSSION

Prior to the first *Gaia* data release, the *Gaia* Universe model snapshot (GUMS) simulated a synthetic catalog of objects that *Gaia* could have potentially observed ([Robin et al. 2012](#)). GUMS simulated that nearly one million quasars would be observed by *Gaia*. Our sample roughly agrees with that number, given that it is about 50% incomplete. However, unlike GUMS, our sample consists of real objects actually detected by *Gaia*.

The Large Quasar Astrometric Catalog (LQAC3; [Souhay et al. 2015](#)), is a collection of 321,957 objects and represents the complete set of already identified quasars as of 2015. While the LQAC3 reliably contains extragalactic objects, the LQAC3-*Gaia* cross-match is dominated by the SDSS footprint. Our catalog has a more uniform sky distribution, and is therefore preferable for the study of low-multipole proper motion signals.

We expect *Gaia*-WISE AGN to be able to measure the secular aberration drift with 23σ significance. [Mignard](#)

(2012) predicted that *Gaia* would detect the secular aberration drift with about 10σ accuracy, assuming $10^4 - 10^5$ quasars observed by *Gaia* with proper motion errors lower than predicted here. Titov et al. (2011) predicted *Gaia* to measure the dipole parameters with about 10% relative precision. We find that the catalog should be able to measure the dipole parameters with higher precision, with the exception of the s_{11}^{Re} component.

While isotropy is a fundamental pillar of cosmology and is well constrained by the cosmic microwave background (Planck Collaboration et al. 2016), *Gaia*-WISE AGN will be able to probe the isotropy of expansion for the relatively local universe since the majority are at redshift below 2.5 (95th percentile value). We predict that *Gaia*-WISE AGN will constrain the anisotropy of the Hubble expansion to about 2%. Darling (2014) showed that the expansion is isotropic to within 7% in the most constrained direction using a catalog of 429 radio sources. Local anisotropy has been previously measured using the Hubble parameters derived from Type Ia supernovae. Chang & Lin (2015) find that the maximum anisotropy of the Hubble parameter is $3\% \pm 1\%$ for a set of supernovae in the redshift range $z < 1.4$. Bengaly (2016) find that the maximum variance of the Hubble parameter is $(2.30 \pm 0.86) \text{ km s}^{-1} \text{ Mpc}^{-1}$ for $z < 0.1$, which corresponds to a maximum departure from isotropy of $3.3\% \pm 1.2\%$. The *Gaia* isotropy measurement will therefore be competitive with and orthogonal to other more traditional methods.

Our analysis of the astrometric signals that may be detected using *Gaia*-WISE AGN has assumed that the proper motions of all objects will be determined with the same precision as point sources. In reality, some galaxies may appear extended to *Gaia*, in which case the precision of the image centroid position will be diminished. The intrinsic variability of AGN will be an additional proper motion noise source, since variable AGN flux can cause the image centroid to move by up to a few mas for nearby AGN (Popović et al. 2012). Microlensing of quasars may also cause the image centroid to shift due to the appearance or disappearance of microimages (Williams & Saha 1995; Lewis & Ibata 1998). The effect on the centroid position may be as large as tens of μas due to stellar mass objects in the lensing galaxy (Treuer & Wambsganss 2004) or a few mas due to stellar clusters (Popović & Simić 2013). The effects of both AGN variability and microlensing will add uncorrelated noise to the proper motions. They will therefore be averaged out in the determination of correlated signals such as the secular aberration drift and anisotropic expansion, despite adding to the overall noise in the signals.

6. CONCLUSIONS

We presented a catalog of *Gaia* AGN selected using the WISE two color method of Mateos et al. (2012). The catalog contains 567,721 objects, and we estimate

that this sample is roughly 50% complete. We find that the WISE wedge reliably selects extragalactic objects, with only a negligible portion (0.2%) of our sample likely contaminated by stars. We demonstrated two potential applications of the catalog, a precise measurement of the secular aberration drift and strong constraints on the isotropy of the Hubble expansion. Based on the expected end-of-mission proper motion uncertainty for each object in the *Gaia*-WISE catalog, we predict a measurement of the secular aberration drift with $\sim 23\sigma$ significance and a limit on the anisotropy of the Hubble flow of $\sim 2\%$.

The authors thank the anonymous referee for helpful feedback.

The authors acknowledge support from the NSF grant AST-1411605 and the NASA grant 14-ATP14-0086.

This work has made use of data from the European Space Agency (ESA) mission *Gaia* (<https://www.cosmos.esa.int>), processed by the *Gaia* Data Processing and Analysis Consortium (DPAC, <https://www.cosmos.esa.int/web/gaia/dpac>). Funding for the DPAC has been provided by national institutions, in particular the institutions participating in the *Gaia* Multilateral Agreement.

This publication makes use of data products from the Wide-field Infrared Survey Explorer, which is a joint project of the University of California, Los Angeles, and the Jet Propulsion Laboratory/California Institute of Technology, funded by the National Aeronautics and Space Administration.

Funding for SDSS-III has been provided by the Alfred P. Sloan Foundation, the Participating Institutions, the National Science Foundation, and the U.S. Department of Energy Office of Science. The SDSS-III web site is <http://www.sdss3.org/>. SDSS-III is managed by the Astrophysical Research Consortium for the Participating Institutions of the SDSS-III Collaboration including the University of Arizona, the Brazilian Participation Group, Brookhaven National Laboratory, Carnegie Mellon University, University of Florida, the French Participation Group, the German Participation Group, Harvard University, the Instituto de Astrofísica de Canarias, the Michigan State/Notre Dame/JINA Participation Group, Johns Hopkins University, Lawrence Berkeley National Laboratory, Max Planck Institute for Astrophysics, Max Planck Institute for Extraterrestrial Physics, New Mexico State University, New York University, Ohio State University, Pennsylvania State University, University of Portsmouth, Princeton University, the Spanish Participation Group, University of Tokyo, University of Utah, Vanderbilt University, University of Virginia, University of Washington, and Yale University.

This research has made use of the NASA/IPAC Extragalactic Database (NED) which is operated by the Jet Propulsion Laboratory, California Institute of Technol-

ogy, under contract with the National Aeronautics and Space Administration.

Software: `astropy` (Astropy Collaboration et al. 2013), `pyGaia`, `STILTS` (Taylor 2006), `TOPCAT` (Taylor 2005)

REFERENCES

- Ahn, C. P., Alexandroff, R., Allende Prieto, C., et al. 2012, *ApJS*, 203, 21
- Alam, S., Albareti, F. D., Allende Prieto, C., et al. 2015, *ApJS*, 219, 12
- Amendola, L., Eggers Bjä lde, O., Valkenburg, W., & Wong, Y. Y. Y. 2013, *JCAP*, 12, 042
- Assef, R. J., Stern, D., Kochanek, C. S., et al. 2013, *ApJ*, 772, 26
- Astropy Collaboration, Robitaille, T. P., Tollerud, E. J., et al. 2013, *A&A*, 558, A33
- Bengaly, C. A. P., Jr. 2016, *JCAP*, 4, 036
- Book, L. G. & Flanagan, É. É. 2011, *Phys. Rev. D*, 83, 024024
- Chang, Z., & Lin, H.-N. 2015, *MNRAS*, 446, 2952
- Darling, J. 2014, *MNRAS*, 442, L66
- Darling, J., Truebenbach, A. E., & Paine, J. 2017, *ApJ*, submitted
- Fontanini, M., West, E. J., & Trodden, M. 2009, *Phys. Rev. D*, 80, 123515
- Gaia Collaboration, Brown, A. G. A., Vallenari, A., et al. 2016, *A&A*, 595, A2
- Gwinn, C. R., Eubanks, T. M., Pyne, T., Birkinshaw, M., & Matsakis, D. N. 1997, *ApJ*, 485, 87
- Kirkpatrick, J. D., Cushing, M. C., Gelino, C. R., et al. 2011, *ApJS*, 197, 19
- Lewis, G. F., & Ibata, R. A. 1998, *ApJ*, 501, 478
- Mainzer, A., Bauer, J., Grav, T., et al. 2011, *ApJ*, 731, 53
- Marrese, P.M., Marinoni, S., Giuffrida, G., and Fabrizio, M. 2017, *A&A*, submitted
- Mateos, S., Alonso-Herrero, A., Carrera, F. J., et al. 2012, *MNRAS*, 426, 3271
- Mignard, F. 2012, *Mem. Soc. Astron. Italiana*, 83, 918
- Mignard, F., & Klioner, S. 2012, *A&A*, 547, A59
- Nikutta, R., Hunt-Walker, N., Nenkova, M., Ivezić, Ž., & Elitzur, M. 2014, *MNRAS*, 442, 3361
- Padovani, P., Alexander, D. M., Assef, R. J., et al. 2017, *A&A Rv*, 25, 2
- Pâris, I., Petitjean, P., Ross, N. P., et al. 2017, *A&A*, 597, A79
- Planck Collaboration, Ade, P. A. R., Aghanim, N., et al. 2016, *A&A*, 594, A16
- Popović, L. Č., Jovanović, P., Stalevski, M., et al. 2012, *A&A*, 538, A107
- Popović, L. Č., & Simić, S. 2013, *MNRAS*, 432, 848
- Quercellini, C., Cabella, P., Amendola, L., Quartin, M., & Balbi, A. 2009, *Phys. Rev. D*, 80, 063527
- Reid, M. J., Menten, K. M., Brunthaler, A., et al. 2014, *ApJ*, 783, 130
- Robin, A. C., Luri, X., Reylé, C., et al. 2012, *A&A*, 543, A100
- Secrest, N. J., Dudik, R. P., Dorland, B. N., et al. 2015, *ApJS*, 221, 12
- Souchay, J., Andrei, A. H., Barache, C., et al. 2015, *A&A*, 583, A75
- Stern, D., Eisenhardt, P., Gorjian, V., et al. 2005, *ApJ*, 631, 163
- Stern, D., Assef, R. J., Benford, D. J., et al. 2012, *ApJ*, 753, 30
- Taylor, M. B. 2005, *Astronomical Data Analysis Software and Systems XIV*, 347, 29
- Taylor, M. B. 2006, *Astronomical Data Analysis Software and Systems XV*, 351, 666
- Titov, O., Lambert, S. B., & Gontier, A.-M. 2011, *A&A*, 529, A91
- Titov, O., & Lambert, S. 2013, *A&A*, 559, A95
- Treyer, M., & Wambsganss, J. 2004, *A&A*, 416, 19
- Truebenbach, A. E., & Darling, J. 2017, *MNRAS*, 468, 196
- Truebenbach, A. E., & Darling, J. 2017, *ApJ*, submitted
- Véron-Cetty, M.-P., & Véron, P. 2010, *A&A*, 518, A10
- Williams, L. L. R., & Saha, P. 1995, *AJ*, 110, 1471
- Wright, E. L., Eisenhardt, P. R. M., Mainzer, A. K., et al. 2010, *AJ*, 140, 1868-1881
- Xu, M. H., Wang, G. L., & Zhao, M. 2012, *A&A*, 544, A135

APPENDIX

A. CATALOG

Table 2 lists the first ten rows of the *Gaia*-WISE extragalactic catalog. The full catalog containing 567,721 objects will be available as a machine-readable table provided by the publisher.

Table 2. *Gaia*-WISE Extragalactic Catalog

<i>Gaia</i> ID	RA	σ_{RA}	Dec	σ_{Dec}	G	<i>ALLWISE</i> ID	W1	σ_{W1}	W2	σ_{W2}	W3	σ_{W3}	Redshift	Proper Motion Uncertainties ^a	
	J2000		J2000											$\sigma_{\mu, RA}$	$\sigma_{\mu, Dec}$
	(degrees)	(mas)	(degrees)	(mas)	(mag)		(mag)	(mag)	(mag)	(mag)	(mag)	(mag)		($\mu\text{as yr}^{-1}$)	($\mu\text{as yr}^{-1}$)
4990063153917291776	0.00026196	0.4	-47.64309208	0.4	18.637	J000000.06-473835.1	14.086	0.027	13.233	0.028	9.987	0.048		81	81
2875546163053982464	0.00062956	2.6	35.51784342	1.0	18.537	J000000.15+353104.1	14.522	0.030	13.372	0.031	10.663	0.102		108	108
2341836724939897216	0.00066058	0.3	-20.07434420	0.3	17.910	J000000.15-200427.7	13.548	0.026	12.539	0.025	9.727	0.053		85	85
4635686437412067840	0.00102928	1.2	-78.53449449	1.4	20.226	J000000.23-783204.1	15.212	0.031	13.694	0.028	10.388	0.055		336	336
2305851255551067776	0.00142474	3.9	-41.49299774	0.6	18.597	J000000.33-412934.9	15.083	0.033	13.881	0.035	10.396	0.060		93	93
2747188660230483712	0.00191760	0.4	9.38565564	0.2	18.234	J000000.46+092308.2	15.316	0.042	14.019	0.044	10.518	0.108		113	113
2420718231737082368	0.00308067	1.2	-13.95693841	1.0	19.833	J000000.73-135724.8	15.894	0.053	14.556	0.058	11.170	0.147		371	371
2341416058663072000	0.00345683	0.4	-21.29793756	0.4	18.551	J000000.82-211752.5	14.668	0.031	13.405	0.032	10.934	0.130		132	132
2744944385199380480	0.00408179	1.3	4.82979136	0.4	19.661	J000000.98+044947.1	15.503	0.044	13.987	0.044	10.764	0.112	1.62	338	338
2746747137592463872	0.00424303	1.8	8.07294561	0.7	20.003	J000001.02+080422.6	15.332	0.042	14.160	0.045	11.118	0.171		441	441

^a *Gaia* expected end-of-mission proper motion uncertainty (see Section 3.5).